In-depth characterization of HINT1 pathogenic variants

Silvia Amor-Barris[1,2#], Tamas Lazar[3,4#], Kristien Peeters[1,2], Shoshana J. Wodak[3*] and Albena Jordanova[1,2,5*]

[1] Molecular Neurogenomics Group, VIB Center for Molecular Neurology, VIB, Antwerp, Belgium

[2] Molecular Neurogenomics Group, Department of Biomedical Sciences, University of Antwerp, Belgium

[3] VIB-VUB Center for Structural Biology, Vlaams Instituut voor Biotechnologie (VIB), Brussels, Belgium

[4] Structural Biology Brussels, Department of Bioengineering, Vrije Universiteit Brussel, Brussels, Belgium

[5] Department of Medical Chemistry and Biochemistry, Medical University - Sofia, Sofia, Bulgaria

[#] Equal contribution

* corresponding authors - email: albena.jordanova@uantwerpen.vib.be, shoshana.wodak@gmail.com

ABSTRACT

Loss-of-function variants in HINT1 were identified to cause axonal recessive peripheral neuropathy with neuromyotonia (NMAN). Patients suffer from motor-greater-than-sensory polyneuropathy with an age of onset, mainly within the first decade of life. Currently, nearly 30 NMAN disease-causing variants have been described, predominantly in sporadic cases and small families, most of them with limited functional evidence of pathogenicity. We systematically characterized all reported pathogenic missense mutations in HINT1, aiming to dissect their underlying loss-of-function mechanism. Individual variants were mapped onto the crystal structure of the HINT1 protein, and their potential effect on protein stability was computed. These variants were grouped into three main clusters: around the catalytic pocket, at the dimer interface, and in the β-sheet behind the catalytic pocket of the protein. The stability and functionality of the corresponding altered proteins were tested *in vivo* using HINT1 KO cells and a yeast model deficient for the orthologous gene (*HNT1*), providing insights into the structure-function relations. Our findings support the pathogenic character of most of the variants and uncover their differential effect on HINT1 function. Classifying the variants in three clusters sets the basis for patient stratification strategies for future therapeutic development.

Keywords: axonal neuropathy, pathogenic variants, variant effect, protein structure, protein stability

INTRODUCTION

Autosomal recessive axonal neuropathy with neuromyotonia (NMAN [MIM:137200]) is caused by the loss of functional histidine triad nucleotide-binding protein 1 (HINT)[1]. NMAN is a rare disorder affecting over 160 families worldwide, with a higher prevalence in Europe. Patients display a motor greater than sensory polyneuropathy with an age of onset mainly within the first decade of life. It is a slowly progressive chronic disease that is currently incurable. Neuromyotonia is a diagnostic hallmark of the disease, present in 70% of the patients and clinically manifesting as a delayed muscle relaxation after a voluntary contraction[1,2].

HINT1 is part of the histidine triad (HIT) superfamily characterized by a highly conserved motif (His-X-Hix-X-His-X-X, where X= hydrophobic amino acid) in the catalytic core near the carboxyl terminus. It forms a dimer that functions enzymatically as a purine phosphoramidase[3-5] and has also been described as a SUMOylase[6]. A total of 55 HINT1 structures are currently deposited in the Protein Data Bank (PDB), including two pathogenic forms (p.Cys84Arg[4,5], and p.His112Asn[4,7]) and co-crystal structures with potential endogenous substrates[8,9]. Moreover, several enzymology studies have dissected its phosphoramidase activity[5,8,10-13]. Despite the vast information available, the endogenous substrate(s) and its biological relevance remain unknown. *In vivo*, HINT1 is a transcriptional regulator involved in apoptosis[14,15], tumor suppression[16,17], and cardiac hypertrophy[18]. In the central nervous system, it affects the endocannabinoid pathway by modulating the NMDAR activity[19-21]. However, its role in the peripheral nervous system remains uncharacterized.

Currently, nearly 30 variants have been associated with NMAN, most occurring in sporadic patients and often in compound-heterozygous states. While protein-truncating variants are clearly detrimental, it is difficult to define the pathogenic potential of missense variants resulting from single residue mutations. It is, therefore, essential to evaluate these NMAN variants and see how they affect HINT1 function and whether there are different routes toward neurotoxicity. In this study, we systematically characterize 22 reported missense variants combining *in silico, in vitro,* and *in vivo* approaches, focusing primarily on the effect of these variants on protein stability and enzymatic activity, the best-defined function of HINT1 so far. Here, we classify variants in three functional and structural clusters based on their structural and functional consequences.

MATERIAL AND METHODS

Solvent accessibility surface area and *in silico* protein fold stability calculations.

We used the Protein Interaction Calculator (PIC[22]) web tool to calculate and characterize different types of intra- and intermolecular residue-residue interactions in the X-ray structure of the WT HINT1 protein (PDB: 5KLZ). All interaction types were calculated by using default parameters offered by the server.

The same X-ray structure was used to calculate the solvent accessible surface area of individual residues (ASA_R) in the monomer and the dimer, respectively, and various related quantities. These included the buried surface area of a residue (BSA_R) upon dimer formation, with BSA_R = [(ASA_R(monomer) – ASA_R(dimer)]; the $fBSA_R$: the surface area fraction of a residue in the monomer that gets buried in the dimer: $fBSA_R$= [BSA_R / ASA_R(monomer)]; the residue relative accessible surface area RSA_R = [ASA_R (monomer or dimer)/ ASA_R(Gly-X-Gly)], where 'x' represents the same residue in the free dipeptide unit. The ASA_R of the residue in the 'x' position of this very flexible dipeptide is taken to represent its ASA in the unfolded state of the protein. The BSA_R may be considered as representing the contribution of the residue to the dimer stability[23]. $fBSA_R$ evaluates the extent to which a residue is buried at the dimer interface, and RSA_R measures the extent to which a residue gets buried upon folding of the isolated monomer or in the dimer, respectively. The various solvent accessible surface area calculations were performed with the software FreeSASA 2.0.3[24] using default parameters.

The effect on protein stability upon mutation was estimated using the methods implemented in FoldX-4[25], SDM[26], mCSM[27], DUET[28], ENCoM[29], and DynaMut[30] using the default settings. These methods combine information from protein sequences, 3D structures, and crude physico-chemical parameters to calculate the change in protein folding free energy ($\Delta\Delta G$). The calculations were carried out on the isolated $HINT1^{WT}$ monomer from the bound conformation and on the homodimer, to evaluate separately the effect of the variants on the stability of individual subunits and the dimer. It should be noted that an important shortcoming of these methods is that they fail to consider changes in the protein backbone conformation that may occur upon variation. However, so far, no significant conformational changes have been revealed in the crystal structures of various HINT1 variants.

Cloning and Creation of HINT1 Expression Plasmids

Yeast and mammalian expression plasmid with human *HINT1* were generated in previous studies[1,31]. The different *HINT1* variants were introduced with site-directed mutagenesis (SDM) using KAPA HiFi (Roche Diagnostics, Basel, CH). Verification of the variants was done by Sanger sequencing.

Yeast Strain and Transformation

S. cerevisiae strain BY8-5c (MATα *ura3-52 his3Δ200 trp1Δ901 lys2-801 suc2-Δ9 leu2-3,112 hnt1Δ::URA3*)[3] was provided by Dr. Brenner, University of Iowa, USA. Yeast cells were cultured in rich (YP) medium supplemented with 2% glucose. Transformation of BY8-5c with the pAG415GPD expression plasmids carrying one of the *HINT1* variants or the human wild-type was done with the LiAc/SS carrier DNA/PEG method[32]. Positive clones were selected in minimal medium without Leucine (SD-Leu) supplemented with 2% glucose.

Spot Assay

Pre-cultures of the different yeast clones were grown overnight in SD-Leu supplemented with glucose. Absorbance was measured and adjusted to an optical density of OD_{600nm}=1. Serial dilutions of each culture were performed, and 5µl were spotted on SD-Leu agar plates supplemented with either 2% glucose or 2% galactose. Plates were incubated for three days at 39ºC.

Cell Line Establishment and Culture

HINT1 HeLa KO cell lines were created using CRISPR/Cas9, as described before[31]. The single guide RNA (sgRNA) sequence conferring target sequence specificity to the CRISPR/Cas9 system was designed using the sgRNA Designer (Broad Institute). The sgRNA with the highest combined rank was selected (CTTTGGGAAGATCATCCGCA), targeting the first exon of HINT1 with a predicted on-target efficacy of 0.6315. Complete KO of HINT1 was validated on the genomic level by Sanger sequencing and on the protein level by immunoblotting.

HeLa cells were grown in high-glucose DMEM (Gibco, Waltham, MA, USA) supplemented with 10% heat-inactivated fetal bovine serum (FBS, Gibco, Waltham, MA, USA), 1% glutamine (Gibco, Waltham, MA, USA) and 1% penicillin/streptomycin (Gibco, Waltham, MA, USA). Cells were cultured at 37ºC and 5% CO_2 in a humidified atmosphere.

Cell Transfection

HeLa cells were transiently transfected using polyethylenimine (PEI) MW25000 (Polysciences, Warrington, PA, USA) with pCAGGAS vector carrying on the HINT1 variant or the human WT. A pCAGGS-MBP was used as an empty vector control. Cells were seeded in a 6-well plate the day before the transfection in a complete medium without antibiotics. When cells reached 70-80% confluency, they were transfected with PEI and 250ng of plasmid.

Immunoblotting

Cells were lysed in RIPA lysis buffer (20 mM Tris-HCl pH=7.4; 150 mM NaCl; 0.1% Nonidet P-40; 0.5% sodium deoxycholate; 0.1% sodium dodecyl sulfate) supplemented with Halt™ Protease Inhibitor Cocktail (ThermoFisher Scientific, Waltham, MA, USA) for 30 min on ice and cleared by centrifugation for 10 min at 14000 RPM. Protein concentration was determined with the Pierce BCA protein assay kit (ThermoFisher Scientific, Waltham, MA, USA) and adjusted to 20µg per sample. Lysates were boiled for five min at 95ºC in reducing Laemmli sample buffer (Bio-Rad, Hercules, CA, USA) supplemented with 100mM 1.4-Dithiothreitol (DTT).

Yeast proteins were extracted following a previously published protocol[31]. Briefly, yeast cells were collected before the stationary phase (OD_{600nm}=1) by centrifugation. Then, cells were washed first with 2.0M LiAc and then 0.4M NaOH for 5 min on ice. Cells were finally boiled for five min at 95ºC in Laemmli sample buffer (Bio-Rad, Hercules, CA, USA) supplemented with 100mM DTT.

Proteins were separated in 4-15% Mini-PROTEAN® TGX Stain Free™ Protein gels (Bio-Rad, Hercules, CA, USA) and transferred to a nitrocellulose membrane (Hybond™-P, GE Healthcare, Chicago, IL, USA) using the semi-dry Trans-Blot® Turbo™ Transfer System (Bio-Rad, Hercules, CA, USA). Membranes were blocked for an hour at room temperature with 5% milk powder diluted in PBS supplemented with 0.1% Tween-20 and then incubated with a primary antibody overnight at 4ºC and one hour with a secondary horseradish peroxidase-conjugated antibody at room temperature. Membranes were developed with Enhanced Chemiluminescence ECL Plus™ (ThermoFisher Scientific, Waltham, MA, USA) and imaged with ImageQuant™ LAS 4000 (GE Healthcare, Chicago, IL, USA). The antibodies used in this study were: polyclonal rabbit anti-human HINT1 antibody (1:1000, Sigma, San Luis, MO, USA), and to demonstrate equal loading mouse monoclonal anti-β-actin antibody (1:5000, Sigma, San Luis, MO, USA), mouse polyclonal anti-α-tubulin antibody (1:5000, Abcam, Cambridge, UK) or mouse polyclonal anti-PKG antibody (1:10.000, Sigma, San Luis, MO, USA).

Dimerization Reaction

Cells were harvested and lysed in 0.2 triethanolamine, pH=8.0 with 0.3 mg/ml of dimethyl adipimidate (DMP, ThermoFisher Scientific, Waltham, MA, USA) for 1 hour with vertical mixing. Lysates were cleared, and protein concentration was measured before immunoblotting.

RESULTS

Mapping and clustering of HINT1 pathogenic variants

The NMAN-causing non-synonymous variants **(Supplementary Table 1)** were mapped on the sequence and 3D structure of HINT1 **(Fig. 1)**. Five variants (p.Phe33*, p.Cys38*, p.His51*, p.Ser61*, p.Gln62*, and p.Gln106*) were excluded from the study since they create an early stop codon (nonsense variant) leading to a truncated and non-functional protein. Using the HINT1 wild-type (WT) crystal structure (PDB:5KLZ), we defined three different clusters of missense variants considering the spatial location of the 16 remaining variants: 1) the catalytic pocket, 2) the dimer interface, 3) distal β-hairpin and nearby loop **(Fig. 1)**. The initial mapping was complemented by calculating the solvent-accessible surface area (ASA) per residue for the monomeric and dimeric forms **(Table 1)**. The difference between the monomeric and dimeric ASA allows the calculation of the buried surface area (BSA) in the dimeric form and, thus, indicates the contribution of each residue to HINT1 dimerization.

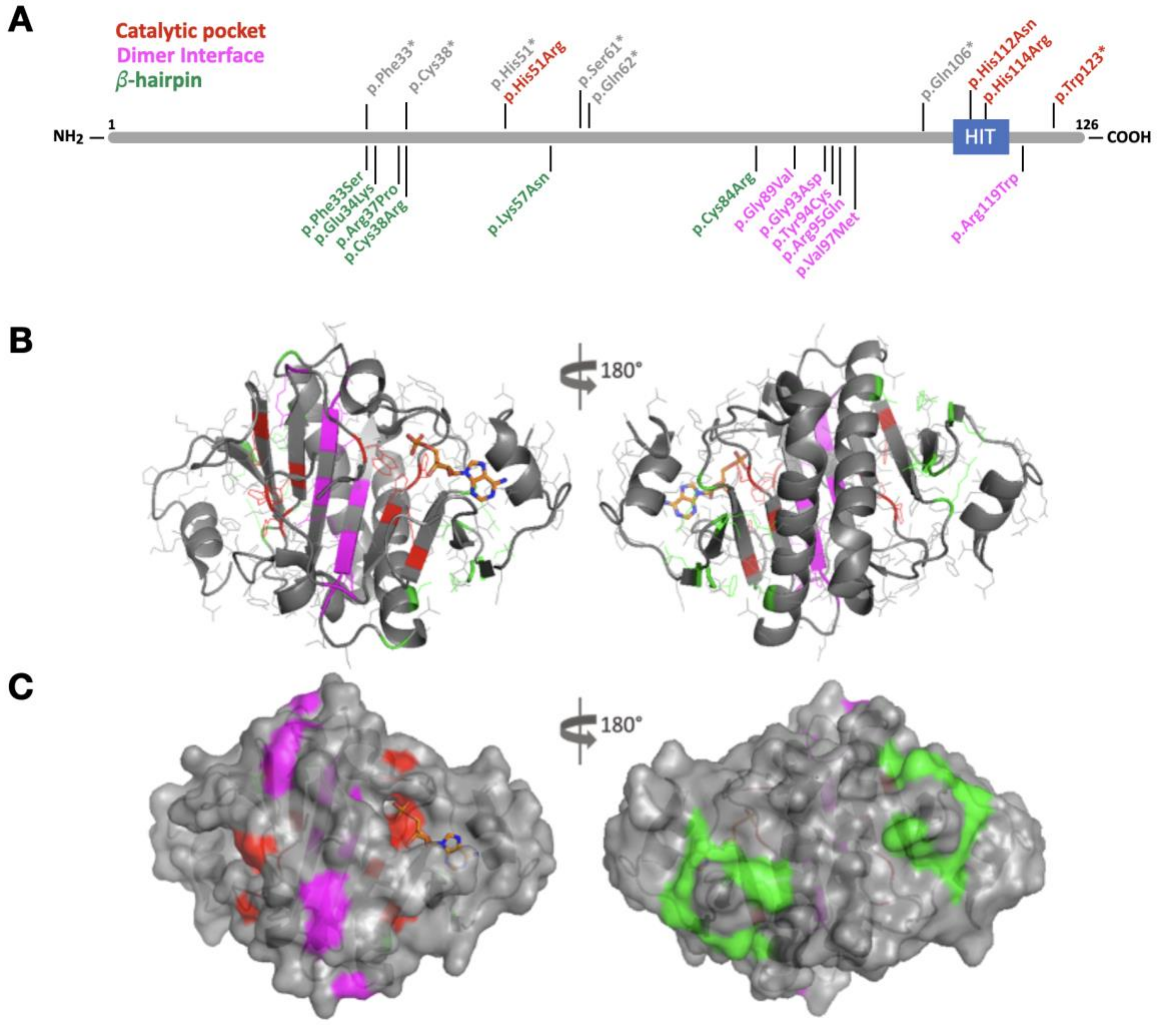

Figure 1. Structural mapping and spatial clustering of the missense NMAN pathogenic variants.

Residues subjected to pathogenic alterations were mapped onto the HINT1 sequence (HIT motif represented as a blue box) **(A)** and dimer **(B, C)** and colored according to the cluster they belong to. Structural mapping (PDB: 5KLZ) of NMAN-causing protein variants is shown in both "cartoon" representations **(B)** and surface representations with moderate transparency **(C)**. The ligand in the binding site is indicated in orange using the "sticks" representation. Red: variants at the catalytic site. Magenta: variants at the dimer interface. Green: variants in the distal β- hairpin and the hairpin-helix region.

The catalytic pocket cluster (**Fig. 1, red**) comprises all the residues involved in the phosphoramidase activity either by being part of the HIT motif (p.His112, p.His114), by stabilizing intermediates (p.His51) or by contributing to substrate recognition (p.Trp123). Additionally, two of the residues (p.His114, p.Trp123) are helping with the stabilization of the dimeric form. The high conservation of these residues across species highlights their important function

(**Supplementary Fig. 1**). The substitution of any of these residues will likely impact the enzymatic process.

The dimer interface cluster (**Fig. 1, magenta**) includes potentially detrimental variants for the dimer formation. These residues form the dimer interface or are near the antiparallel β -sheet that extends across the HINT1 dimer (p.Gly89Val, p.Gly93Asp, p.Tyr94Cys, p.Arg95Gln, p.Val97Met)]. An additional residue (p.Arg119Trp) forms hydrogen bonds with the C-terminus of the neighboring subunit, thereby further stabilizing the contacts between the two protomers. Most residues of this cluster bury a sizable solvent-accessible surface area upon formation of the HINT1 wild-type (WT) dimer (*see Methods for detail*), and significantly more than any of the other analyzed variants (BSA_R in **Table 1**), confirming their important contribution to the dimer interface integrity. Their substitution with polar or bulkier residues is expected to disrupt the dimer interface, thereby abrogating catalytic activity and destabilizing the protein. Although p.Gly89 does not directly contribute to the dimer interface area (**Table 1**), its substitution with Val, a hydrophobic residue, will likely modify the loop before the antiparallel sheet forming the dimer interface and impact stability. The residues of this cluster are conserved, with higher conservation seen for p.Tyr94 and p.Arg119 (**Supplementary Fig. 1)**.

The third cluster includes variants situated far from the dimer interface and the catalytic pocket. They are located at the surface of the protein, featuring the smallest fraction of buried surface area **(Table 1).** Four residues (p.Phe33Ser, p.Glu34Lys, p.Arg37Pro, p.Cys38Arg) are positioned in a β -hairpin at the N-terminus. Two other residues are either adjacent to the β -hairpin (p.Lys57Asn) or in an α-helix that packs against the β-sheet formed by the hairpin (p.Cys84Arg). This cluster contributes to preserving the native helix-sheet interactions (**Fig.1, green**). Interestingly, this part of the protein has the lowest degree of homology among species, with significant conservation only seen among mammals (**Supplementary Fig. 1**)

Table 1: Solvent-accessible surface area and buried area of HINT1 residues undergoing pathogenic alterations in each clusters.

Cluster	Residue	ASA_R dimer (Å^2)	ASA_R monomer (Å^2)	BSA_R (Å^2)	$fBSA_R$	RSA_R dimer (%)	RSA_R monomer (%)
Catalytic Pocket	p.His51	4.65	8.21	3.56	0.43	2.50	4.50
	p.His112	14.94	14.94	0.00	0.00	8.20	8.20
	p.His114	11.80	26.85	15.05	0.56	6.40	14.70
Dimer Interface	p.Gly89	50.01	50.01	0.00	0.00	61.70	61.70
	p.Gly93	3.73	36.08	32.35	0.90	4.60	44.50
	p.Tyr94	5.50	87.36	81.86	0.94	2.60	40.80
	p.Arg95	0.61	50.70	50.09	0.99	2.60	21.30
	p.Val97	0.43	42.66	42.23	0.99	0.30	28.10
	p.Arg119	66.10	108.49	42.39	0.39	27.80	45.60
β-hairpin	p.Phe33	80.15	80.15	0.00	0.00	40.10	40.10
	p.Glu34	72.87	72.87	0.00	0.00	41.80	41.80
	p.Arg37	88.24	101.65	13.41	0.13	37.00	42.70
	p.Cys38	0.00	0.00	0.00	0.00	0.00	0.00
	p.Lys57	51.61	51.61	0.00	0.00	25.20	25.20
	p.Cys84	4.54	4.54	0.00	0.00	3.40	3.40

For the definitions of ASA_R, BSA_R, $fBSA_R$, and RSA_R (monomer) and RSA_R (dimer) see *Methods*. All the values were computed using the 3D structure of $HINT1^{WT}$ (PDB: 5KLZ).

Predicting the effects of the disease-causing variants by computational approaches

To estimate the impact of the variant on protein stability, we applied several computational methods (FoldX-4[17], SDM[18], mCSM[19], DUET[20], ENCoM[16], and DynaMut[21]) to the residues in the HINT1 monomer and dimer, respectively. The distributions of the free energy changes (ΔΔG) computed using the different tools for the monomer and the dimer, respectively, are displayed in **Fig. 2**. Values calculated by FoldX showed the most significant fluctuations, often differing from those of other methods, and were therefore excluded from the distributions (for ΔΔG values computed by all methods, see **Supplementary Table 2**).

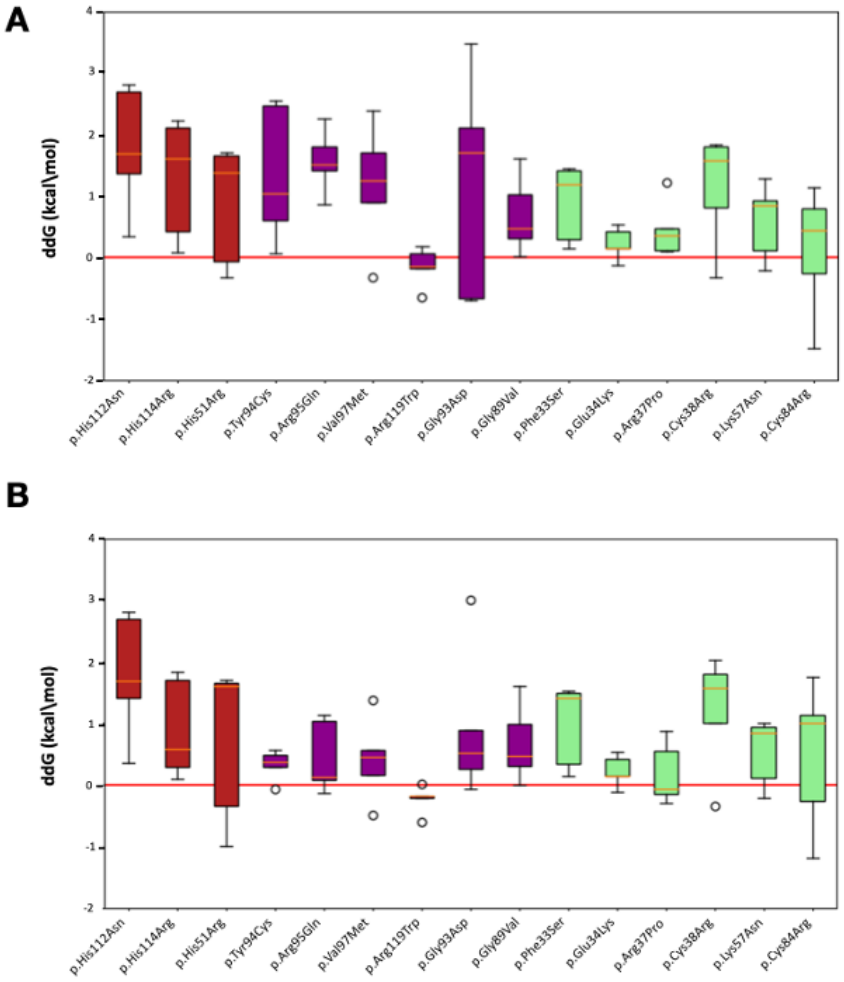

Figure 2: Predicted destabilization effects of the HINT1 missense NMAN variants.

Consensus prediction of the effect of mutations on the HINT1 dimer **(A)** and monomer **(B)** stability. PDB structure 5KLZ chain A+B was used as input for evaluating the effects on dimer stability, and chain B alone for monomer stability. The ΔΔG distributions represent the ΔΔG values obtained using the different stability predictors (*see Materials & Methods for details*).

Results show that the catalytic cluster variants, p.His51Arg, p.His112Asn, p.His114Arg, are predicted to destabilize the monomer and dimer similarly, indicating that monomer destabilization is their main effect. This suggests that these variants may also affect protein stability and interfere with catalytic activity. Except for p.Arg119Trp, all the disease-causing variants of residues in the dimer interface cluster (p.Gly93Asp, p.Tyr94Cys, p.Arg95Gln, p.Val97Met) are predicted to destabilize the dimer more than the monomer (**Fig. 2A, B**), (by ~1-1.5 kcal/mol). Interestingly, the p.Gly93Asp mutation is predicted to cause the most severe dimer destabilization (+3.0 kcal/mol)

by all methods. The pathogenic variants of the β-hairpin cluster are predicted to have only mild destabilizing effects on the dimer and monomer for p.Phe33Ser, p.Glu34Lys, p.Lys57Asn and p.Cys84Arg. The higher destabilizing effect is predicted for the p.Cys38Arg. Only p.Arg37Pro is predicted to marginally impact the stability of the protein (**Fig. 2**).

In vivo characterization of NMAN-pathogenic variants

To assess the pathogenicity of HINT1 variants experimentally, we introduced them into two different systems: *HINT1* knock-out HeLa cell lines created using CRISPR/Cas9 genome editing technology and a *HNT1* knock-out yeast strain (BY8-5c). All the variants were ectopically expressed, and the corresponding proteins were quantified by immunoblotting in both cell systems (**Fig. 3A, B**). The functional impact of each variant was validated by their capability to restore yeast growth under stress conditions (galactose, 39ºC) (**Fig. 3C**).

For the catalytic pocket, only p.His112Asn could be detected by immunoblotting when transiently expressed in HeLa cells (**Fig. 3A**). This aligns with previous reports showing similar stability and structure of the variant compared to the WT protein[1]. However, all the variants could be detected in yeast with only lower levels of p.His51Arg (and, to a lesser extent, p.Trp123*) (**Fig. 3B**). Despite the presence of protein in yeast, none of the variants could rescue the growth deficiency, suggesting a loss of enzymatic function (**Fig. 3C**).

The six variants of the dimer interface cluster had different impacts on the overall stability of the protein in HeLa cells (**Fig. 3A**). Two variants (p.Val97Met, p.Arg119Trp) heavily impacted HINT1 stability. Two others (p.Gly93Asp, p.Arg95Gln) displayed only a reduction in protein expression levels, whereas the last two variants (p.Gly89Val and p.Tyr94Cys) were expressed at levels similar to that of the WT protein. In yeast, however, all the variants were expressed at similar levels to the WT protein, except for p.Val97Met, whose expression was slightly reduced (**Fig. 3B**). Despite all the corresponding proteins being stably expressed in yeast, only p.Gly89Val produced a complete rescue of the HINT1 phenotype, whereas p.Tyr94Cys and p.Arg119Trp enabled only partial recovery, as measured by yeast growth under the tested stress conditions. The remaining three variants (p.Gly93Asp, p.Arg95Gln, p.Val97Met) could not detectably restore yeast growth, confirming their loss of function.

Variants of the β -hairpin cluster were highly unstable in our experiments. In HeLa cells, only the p.Phe33Ser protein was expressed at similar levels as the WT protein, whereas mere traces of the p.Lys57Asn and p.Cys84Arg proteins could be detected by immunoblotting (**Fig. 3A**). The unstable non-native state of these variants was also apparent in yeast, except for the p.Glu34Lys variant, which, although highly unstable in HeLa cells, was stably expressed in yeast (**Fig. 3B**). Furthermore, most variants of this cluster displayed some correlation between their yeast expression level and their ability to complement the *HNT1* deficiency. The p.Phe33Ser and p.Glu34Lys proteins were stably expressed and restored the growth deficiency in yeast as efficiently as the WT protein (**Fig. 3C**). The p.Cys84Arg and p.Lys57Asn proteins, expressed at lower levels in yeast, displayed only partial rescue of the growth phenotype, whereas the remaining variants were highly unstable with barely detectable expression and exhibited no phenotype rescue.

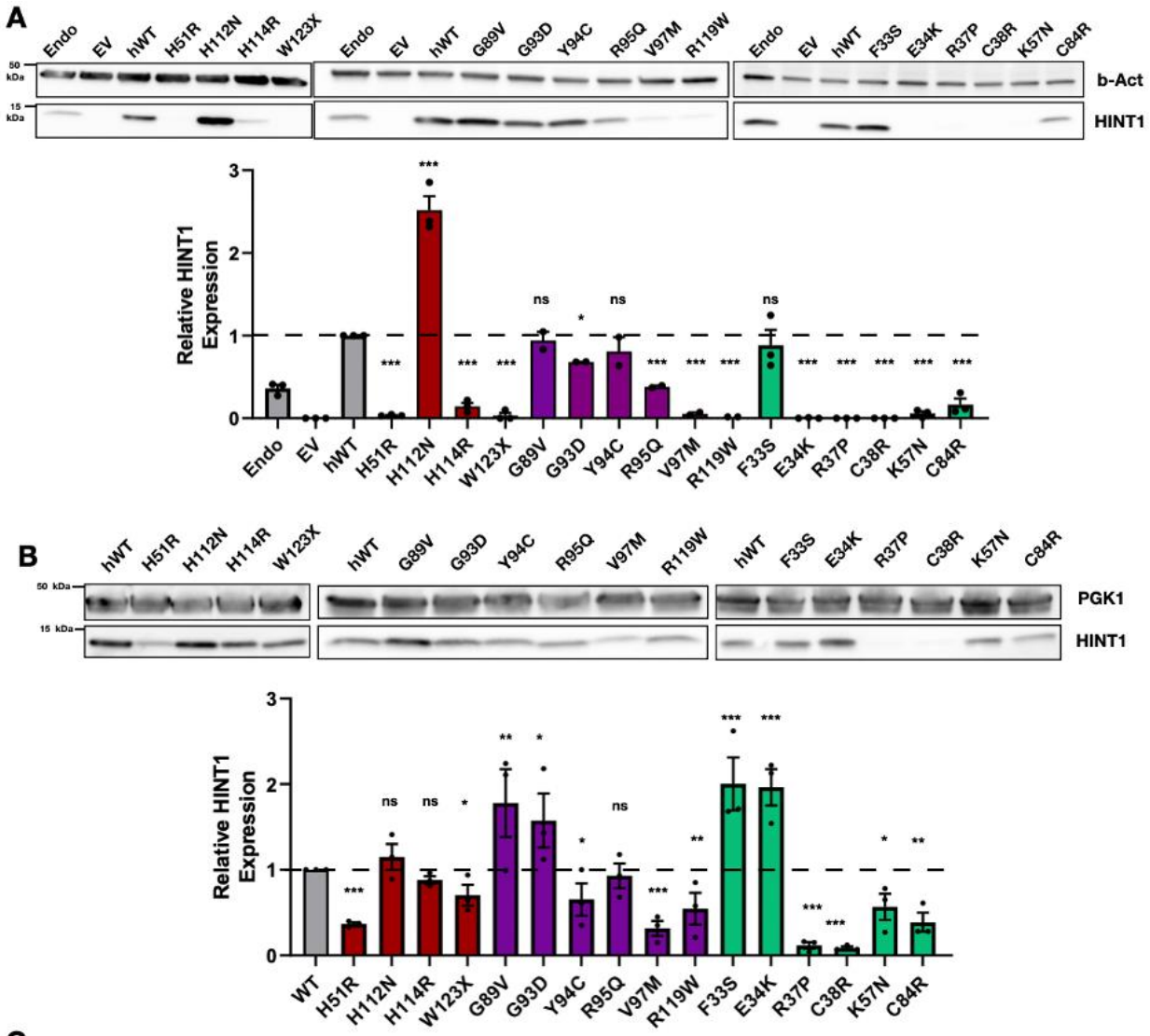
A
Endo
EV
hWT
H51R
H112N
H114R
W123X
G89V
G93D
Y94C
R95Q
V97M
R119W
F33S
E34K
R37P
C38R
K57N
C84R
50 kDa
15 kDa
b-Act
HINT1
Relative HINT1 Expression
B
PGK1
WT
C
OD600
D
25 kDa
dimer
monomer

Figure 3: In vivo characterization of HINT1 variants. **(A)** Each mutant was transiently expressed in HeLa *HINT1* KO cells, and the HINT1 protein levels were assessed by immunoblotting. Equal loading was validated with mouse monoclonal anti- β-actin antibodies, and relative HINT1 expression was normalized to WT expression. The graph represents the relative quantification of band intensities for three independent replicates **(B)** Immunoblotting analysis of protein extracts of a yeast strain expressing the human mutants and WT proteins. Relative quantification of HINT1 levels was normalized to the expression of hWT protein. **(C)** Genetic complementation analysis in a *HNT1*-deleted yeast strain. A serial dilution of yeast cultured was spotted in a plate and let it grow for three days under stress conditions (2% Galactose, 39ºC). **(D)** Immunoblotting after dimerization reaction using DMP. HINT1 protein expression levels in monomeric (14 kDa) and dimeric (28 kDa) could be detected. Statistical one-way ANOVA was used in all western-blot quantifications. Bar charts are presented as means with standard error of the mean (s.e.m). ns = no significant, *p<0.05, **p<0.01, *** p<0.001

HINT1 enzymatic function is directly linked to the ability of the protein to form homodimers. It is, therefore, interesting to investigate the dimer formation capability of the stably expressed variants. To this end, we transiently expressed the variants of interest in the HeLa KO cell lines and treated the lysates with dimethyl pimelimidate (DMP), a cross-linker reagent active towards primary amines. It has a short linker (7 Å), allowing the study of protein quaternary structures by covalently binding the different subunits together. Protein levels of the monomer and the dimer were detected via immunoblotting (**Fig. 3D**). In cells expressing WT proteins, two bands were detected, one around 14 kDa and another around 28 kDa, corresponding to the monomer and the dimer, respectively. A range of behaviors was observed for the tested variants (**Fig. 3D**). Only the p.Gly89Val mutant could form dimers similar to the WT protein. Two variants (p.Phe33Ser, p.His112Asn) showed a weight shift of the dimer species but not of the monomer. This shift was significantly larger for the p.His112Asn mutant, suggesting that a potential additional binding partner was cross-linked. One variant (p.Tyr94Cys) exhibited several bands, indicating that it either interacts with other partners or aggregates. Finally, only the p.Gly93Asp variant appeared to remain monomeric.

DISCUSSION

NMAN is a rare disease caused by more than 20 pathogenic variants spread across the protein. Most of them have been identified in single families or isolated patients and often in compound heterozygous states with limited functional evidence of pathogenicity. Overall, there is *in vivo* data for only one-fourth of all HINT1 pathogenic variants[1,31,33], while the impact of the rest of the

variants has only been partially assessed *in vitro*[6,7]. Obtaining biological samples from the patients is not always possible, highlighting the need for standardized assays to test pathogenicity.

We used a systematic combined approach using *in silico,* cell-based, and *in vivo* assays to characterize all missense variants, providing information on how the variant impacts HINT1 stability and function. The *in silico* mutational analysis involved mapping the positions undergoing mutation onto the HINT1 X-ray structure (**Fig. 1**) and producing rough estimates of the effect of the variants on the monomer and dimer folding free energies (stability) (**Fig. 2**). In addition, we also carried out solvent accessibility calculations, which estimate contributions to protein stability due to desolvation effects (**Table 1**). Taken together, these analyses allowed us to group the residues undergoing mutations into three main clusters based on the location of the variants within the structure (**Fig. 1**), infer their impact on the monomer, the dimer, and the enzymatic activity, and make a crude assessment of how detrimental a pathogenic variant is.

Aware of the limitations of this type of *in silico* analysis, which also fails to consider the native biological context, the theoretical studies were complemented by cellular assays (**Fig. 3**). In HeLa cells, the stability of the pathogenic variants can be accurately tested under physiological conditions, but not their functionality. Therefore, function, or loss of function, was further evaluated in yeast (**Fig. 3**). This was further justified by previous reports showing that protein stability can differ between the two cellular systems[31,33]. The stability studies in both HeLa and yeast cells showed that p.Arg37Pro, p.Cys38Arg, p.His51Arg, and p.Val97Met were highly unstable (**Fig. 3A**). The low stability of the p.Arg37Pro HINT1 variant was further demonstrated by our unsuccessful attempts to purify it in a soluble state. These observations align with previous reports on the difficulty of recombinantly producing and purifying the p.Arg37Pro, and p.His51Arg variants[7]. Interestingly, the p.Arg37Pro variant was predicted to destabilize the structure of the monomer only mildly, probably because the *in silico* methods do not take into account the effect that replacing an arginine residue by the more conformationally constrained proline may have on the backbone conformation of the protein. Such inconsistencies between *in silico* and *in vivo* experiments reinforce the use of combinatorial approaches to define the detrimental effects of pathogenic variants.

After the systematic characterization, we could not conclude the pathogenicity of two variants (p.Gly89Val and p.Phe33Ser). The assays we used are limited to study the stability of the protein and its enzymatic activity. Therefore, these variants may disrupt other HINT1 functions or

interactions, as suggested in previous *in vitro* studies[6,34]. The description of a new enzymatic activity (SUMOylase) questions whether both enzymatic activities are conserved in yeast, giving a potential explanation for the apparent functionality of the variants; however, whether HINT1 would act as SUMOylase *in vivo* needs to be clarified. Although these two variants appeared to be non-pathogenic in our assays, the genetic and clinical evidence strongly supports their pathogenic character[1]. These variants are, therefore, of interest for elucidating which of the many functions of HINT1 is involved in peripheral neuropathy.

Discrepancies emerged for certain variants (p.Glu34Lys, p.Cys84Arg, p.Arg95Gln): although some protein variants are degraded in HeLa, they remain detectable in yeast (**Figure 3A-B**). These differences can be partially explained by the protein expression systems used. HeLa cells were transiently transfected with a mammalian expression vector, while the yeast cells were stably expressing HINT1 proteins from a multicopy yeast expression vector. This could lead to multiple copies of the same construct per yeast cell and thus increase the amount of protein produced even further. Additionally, an extensive study on the meltome of different organisms showed that the optimal growth temperature for each organism influences the average melting temperatures of its proteome[35]. This would support the idea that culturing the yeast at lower temperatures might help stabilize the altered proteins.

The higher stability of the altered proteins in yeast allowed for testing the functionality of these otherwise degraded variants (**Fig. 3C**). We identified variants that keep some enzymatic activity despite being degraded in mammalian cells (p.Glu34Lys, p.Cys84Arg). Previous *in vitro* studies showed a similar behavior where variants mildly affecting the HINT1 structure retained their enzymatic activity (p.Cys84Arg, p.Gly89Val)[4]. In our assays, this appeared to be a common theme among variants of the β -hairpin cluster, where a correlation existed between protein expression in yeast and growth recovery. Therefore, we hypothesized these variants would be good candidates for developing a pharmacochaperone drug. This approach was followed successfully to treat cystic fibrosis with a channel stabilizer[36].

The classification of all NMAN variants in three different groups based on their molecular characteristics can be used in the future as a base for a patient stratification strategy. Using the developed assays as a standard, the impact of new pathogenic variants on the HINT1 function could be dissected, and the best treatment approach could be chosen accordingly.

CONFLICT OF INTEREST

The authors declare that they do not have any conflict of interest.

ACKNOWLEDGEMENTS AND FUNDING

This study was funded by the Research Foundation-Flanders (FWO): Research grants G049217N and #G0A2122N (to A.J.); Postdoctoral fellowship to K.P.; Pre-doctoral fellowship to S.A.B. The AFMTELETHON: research grant 23708 (to A.J.), Trampoline grant to K.P.

T.L. is a postdoctoral innovation mandate holder (HBC.2022.0194) of the Flanders Innovation & Entrepreneurship Agency (VLAIO).

REFERENCES

1 Zimon, M. *et al.* Loss-of-function mutations in HINT1 cause axonal neuropathy with neuromyotonia. *Nat Genet* **44**, 1080-1083 (2012). https://doi.org:10.1038/ng.2406

2 Peeters, K., Chamova, T., Tournev, I. & Jordanova, A. Axonal neuropathy with neuromyotonia: there is a HINT. *Brain* **140**, 868-877 (2017). https://doi.org:10.1093/brain/aww301

3 Bieganowski, P. *et al.* Adenosine monophosphoramidase activity of Hint and Hnt1 supports function of Kin28, Ccl1, and Tfb3. *J Biol Chem* **277**, 10852-10860 (2002). https://doi.org:10.1074/jbc.M111480200

4 Shah, R., Maize, K. M., Zhou, X., Finzel, B. C. & Wagner, C. R. Caught before Released: Structural Mapping of the Reaction Trajectory for the Sofosbuvir Activating Enzyme, Human Histidine Triad Nucleotide Binding Protein 1 (hHint1). *Biochemistry* **56**, 3559-3570 (2017). https://doi.org:10.1021/acs.biochem.7b00148

5 Zhou, X. *et al.* Kinetic mechanism of human histidine triad nucleotide binding protein 1. *Biochemistry* **52**, 3588-3600 (2013). https://doi.org:10.1021/bi301616c

6 Cortes-Montero, E., Rodriguez-Munoz, M., Sanchez-Blazquez, P. & Garzon-Nino, J. Human HINT1 Mutant Proteins that Cause Axonal Motor Neuropathy Exhibit Anomalous Interactions with Partner Proteins. *Mol Neurobiol* (2021). https://doi.org:10.1007/s12035-020-02265-x

7 Shah, R. M. *et al.* Structure and Functional Characterization of Human Histidine Triad Nucleotide-Binding Protein 1 Mutations Associated with Inherited Axonal Neuropathy with Neuromyotonia. *J Mol Biol* **430**, 2709-2721 (2018). https://doi.org:10.1016/j.jmb.2018.05.028

8 Maize, K. M. *et al.* A Crystal Structure Based Guide to the Design of Human Histidine Triad Nucleotide Binding Protein 1 (hHint1) Activated ProTides. *Mol Pharm* **14**, 3987-3997 (2017). https://doi.org:10.1021/acs.molpharmaceut.7b00664

9 Shah, R. *et al.* Inhibition by divalent metal ions of human histidine triad nucleotide binding protein1 (hHint1), a regulator of opioid analgesia and neuropathic pain. *Biochem Biophys Res Commun* **491**, 760-766 (2017). https://doi.org:10.1016/j.bbrc.2017.07.111

10 Zhou, X. *et al.* Kinetic Mechanism of Human Histidine Triad Nucleotide Binding Protein 1. *Biochemistry* **52**, 3588-3600 (2013). https://doi.org:10.1021/61301616c

11 Bardaweel, S., Pace, J., Chou, T. F., Cody, V. & Wagner, C. R. Probing the impact of the echinT C-terminal domain on structure and catalysis. *J Mol Biol* **404**, 627-638 (2010). https://doi.org:10.1016/j.jmb.2010.09.066

12 Chou, T. F. *et al.* Engineered monomeric human histidine triad nucleotide-binding protein 1 hydrolyzes fluorogenic acyl-adenylate and lysyl-tRNA synthetase-generated lysyl-adenylate. *J Biol Chem* **282**, 15137-15147 (2007). https://doi.org:10.1074/jbc.M606972200

13 Chou, T. F., Sham, Y. Y. & Wagner, C. R. Impact of the C-terminal loop of histidine triad nucleotide binding protein1 (Hint1) on substrate specificity. *Biochemistry* **46**, 13074-13079 (2007). https://doi.org:10.1021/bi701244h

14 Duan, D. D. *et al.* Hint1 Overexpression Inhibits the Cell Cycle and Induces Cell Apoptosis in Human Osteosarcoma Cells. *Onco Targets Ther* **13**, 8223-8232 (2020). https://doi.org:10.2147/OTT.S242344

15 Weiske, J. & Huber, O. The histidine triad protein Hint1 triggers apoptosis independent of its enzymatic activity. *J Biol Chem* **281**, 27356-27366 (2006). https://doi.org:10.1074/jbc.M513452200

16 Wu, X. S. *et al.* Hint1 suppresses migration and invasion of hepatocellular carcinoma cells in vitro by modulating girdin activity. *Tumour Biol* **37**, 14711-14719 (2016). https://doi.org:10.1007/s13277-016-5336-z

17 Genovese, G. *et al.* The tumor suppressor HINT1 regulates MITF and beta-catenin transcriptional activity in melanoma cells. *Cell Cycle* **11**, 2206-2215 (2012). https://doi.org:10.4161/cc.20765

18 Zhang, Y. *et al.* HINT1 (Histidine Triad Nucleotide-Binding Protein 1) Attenuates Cardiac Hypertrophy Via Suppressing HOXA5 (Homeobox A5) Expression. *Circulation* **144**, 638-654 (2021). https://doi.org:10.1161/CIRCULATIONAHA.120.051094

19 Rodriguez-Munoz, M. *et al.* The sigma1 receptor engages the redox-regulated HINT1 protein to bring opioid analgesia under NMDA receptor negative control. *Antioxid Redox Signal* **22**, 799-818 (2015). https://doi.org:10.1089/ars.2014.5993

20 Garzon, J. *et al.* HINT1 protein: a new therapeutic target to enhance opioid antinociception and block mechanical allodynia. *Neuropharmacology* **89**, 412-423 (2015). https://doi.org:10.1016/j.neuropharm.2014.10.022

21 Rodriguez-Munoz, M., Cortes-Montero, E., Pozo-Rodrigalvarez, A., Sanchez-Blazquez, P. & Garzon-Nino, J. The ON:OFF switch, sigma1R-HINT1 protein, controls GPCR-NMDA receptor cross-regulation: implications in neurological disorders. *Oncotarget* **6**, 35458-35477 (2015). https://doi.org:10.18632/oncotarget.6064

22 Tina, K. G., Bhadra, R. & Srinivasan, N. PIC: Protein Interactions Calculator. *Nucleic Acids Res* **35**, W473-476 (2007). https://doi.org:10.1093/nar/gkm423

23 Janin, J. Principles of protein-protein recognition from structure to thermodynamics. *Biochimie* **77**, 497-505 (1995). https://doi.org:10.1016/0300-9084(96)88166-1

24 Mitternacht, S. FreeSASA: An open source C library for solvent accessible surface area calculations. *F1000Res* **5**, 189 (2016). https://doi.org:10.12688/f1000research.7931.1

25 Schymkowitz, J. *et al.* The FoldX web server: an online force field. *Nucleic Acids Res* **33**, W382-388 (2005). https://doi.org:10.1093/nar/gki387

26 Worth, C. L., Preissner, R. & Blundell, T. L. SDM--a server for predicting effects of mutations on protein stability and malfunction. *Nucleic Acids Res* **39**, W215-222 (2011). https://doi.org:10.1093/nar/gkr363

27 Pires, D. E., Ascher, D. B. & Blundell, T. L. mCSM: predicting the effects of mutations in proteins using graph-based signatures. *Bioinformatics* **30**, 335-342 (2014). https://doi.org:10.1093/bioinformatics/btt691

28 Pires, D. E., Ascher, D. B. & Blundell, T. L. DUET: a server for predicting effects of mutations on protein stability using an integrated computational approach. *Nucleic Acids Res* **42**, W314-319 (2014). https://doi.org:10.1093/nar/gku411

29 Frappier, V., Chartier, M. & Najmanovich, R. J. ENCoM server: exploring protein conformational space and the effect of mutations on protein function and stability. *Nucleic Acids Res* **43**, W395-400 (2015). https://doi.org:10.1093/nar/gkv343

30 Rodrigues, C. H., Pires, D. E. & Ascher, D. B. DynaMut: predicting the impact of mutations on protein conformation, flexibility and stability. *Nucleic Acids Res* **46**, W350-W355 (2018). https://doi.org:10.1093/nar/gky300

31 Amor-Barris, S. *et al.* HINT1 neuropathy in Norway: clinical, genetic and functional profiling. *Orphanet J Rare Dis* **16**, 116 (2021). https://doi.org:10.1186/s13023-021-01746-z

32 Gietz, R. D. & Schiestl, R. H. High-efficiency yeast transformation using the LiAc/SS carrier DNA/PEG method. *Nat Protoc* **2**, 31-34 (2007). https://doi.org:10.1038/nprot.2007.13

33 Malcorps, M. *et al.* HINT1 neuropathy in Lithuania: clinical, genetic, and functional profiling. *Orphanet J Rare Dis* **17**, 374 (2022). https://doi.org:10.1186/s13023-022-02541-0

34 Cortes-Montero, E., Rodriguez-Munoz, M., Sanchez-Blazquez, P. & Garzon, J. The Axonal Motor Neuropathy-Related HINT1 Protein Is a Zinc- and Calmodulin-Regulated Cysteine SUMO Protease. *Antioxid Redox Signal* **31**, 503-520 (2019). https://doi.org:10.1089/ars.2019.7724

35 Jarzab, A. *et al.* Meltome atlas-thermal proteome stability across the tree of life. *Nat Methods* **17**, 495-503 (2020). https://doi.org:10.1038/s41592-020-0801-4

36 Li, H., Pesce, E., Sheppard, D. N., Singh, A. K. & Pedemonte, N. Therapeutic approaches to CFTR dysfunction: From discovery to drug development. *J Cyst Fibros* **17**, S14-S21 (2018). https://doi.org:10.1016/j.jcf.2017.08.013